Supramolecular Architectures on Surfaces Formed through Hydrogen Bonding Optimized in Three Dimensions

Miao Yu,[†] Nataliya Kalashnyk,[†] Wei Xu,[†] Régis Barattin,[‡,§] Youness Benjalal,[∥] Erik Lægsgaard,[†] Ivan Stensgaard,[†] Mohamed Hliwa,[‡,∥] Xavier Bouju,[‡,§] André Gourdon,[‡,§] Christian Joachim,[‡,§] Flemming Besenbacher,[†,*] and Trolle R. Linderoth[†,*]

[†]Interdisciplinary Nanoscience Center (iNANO) and Department of Physics and Astronomy Aarhus University, 8000 Aarhus, Denmark, [‡]CNRS, CEMES, Nanosciences group, 29 rue Jeanne Marvig, 31055 Toulouse, France, [§]Université de Toulouse, UPS, 29 rue Jeanne Marvig, 31055 Toulouse, France, and [∥]Faculté des Sciences Ben M'Sik, Université Hassan II-Mohammédia, Sidi Othman, Casablanca, BP 7955, Morocco

S elf-assembly directed by noncovalent interactions, for example, hydrogen bonding, metal−organic coordination, and van der Waals (vdW) forces, is an extremely versatile approach for the bottom-up fabrication of supramolecular architectures on inorganic solid surfaces, which is expected to be of substantial importance within the emerging field of nanotechnology and nanodevices.[1,2] Numerous hydrogen-bonded one-dimensional (1-D) molecular line and two-dimensional (2-D) network structures grown by molecular self-assembly on surfaces have by now been extensively studied, in particular, by the technique of scanning tunneling microscopy (STM).[3−16] In the majority of cases this has involved planar compounds confined directly onto surfaces in a planar geometry and equipped with structurally rigid chemical functionalities to direct the self-assembly.[3−16] In contrast, so-called "Lander-type" molecules are a special class of compounds in which an aromatic molecular backboard is equipped with bulky chemical side groups which act as spacer legs, providing a pronounced three-dimensional (3-D) structure and decoupling the central aromatic board from the underlying substrate.[17−31] Individual Lander molecules adsorbed on surfaces have previously been demonstrated to have a number of interesting properties, such as altered diffusion behavior,[17] controlled electronic coupling to step edges,[18−21] intramolecular deformation,[21−23] and the ability to act as molds for metallic nanostructures.[22,24−27] Organized 1-D structures of Lander molecules have been formed by adsorption onto surface templates provided by metal-oxide nanogratings[28] or guided by strong molecule−substrate interactions,[29,30,32] but more complex 2-D long-range ordered structures of Lander molecules have not been achieved so far. A program to study the organization and steering of Lander molecules by complementary hydrogen bonding interactions, which is expected to provide a wider variability and control of the structures formed, has therefore been initiated by us.

Here we focus on a specially designed and synthesized Lander molecule equipped with dual diamino-triazine (DAT) functional moieties, enabling these Lander-DAT molecules to interact through mutual,

ABSTRACT Supramolecular self-assembly on surfaces, guided by hydrogen bonding interactions, has been widely studied, most often involving planar compounds confined directly onto surfaces in a planar two-dimensional (2-D) geometry and equipped with structurally rigid chemical functionalities to direct the self-assembly. In contrast, so-called molecular Landers are a class of compounds that exhibit a pronounced three-dimensional (3-D) structure once adsorbed on surfaces, arising from a molecular backboard equipped with bulky groups which act as spacer legs. Here we demonstrate the first examples of extended, hydrogen-bonded surface architectures formed from molecular Landers. Using high-resolution scanning tunnelling microscopy (STM) under well controlled ultrahigh vacuum conditions we characterize both one-dimensional (1-D) chains as well as five distinct long-range ordered 2-D supramolecular networks formed on a Au(111) surface from a specially designed Lander molecule equipped with dual diamino-triazine (DAT) functional moieties, enabling complementary NH · · · N hydrogen bonding. Most interestingly, comparison of experimental results to STM image calculations and molecular mechanics structural modeling demonstrates that the observed molecular Lander-DAT structures can be rationalized through characteristic intermolecular hydrogen bonding coupling motifs which would not have been possible in purely planar 2-D surface assembly because they involve pronounced 3-D optimization of the bonding configurations. The described 1-D and 2-D patterns of Lander-DAT molecules may potentially be used as extended molecular molds for the nucleation and growth of complex metallic nanostructures.

KEYWORDS: hydrogen bonding · self-assembly · molecular modeling · scanning tunneling microscopy · Lander molecule
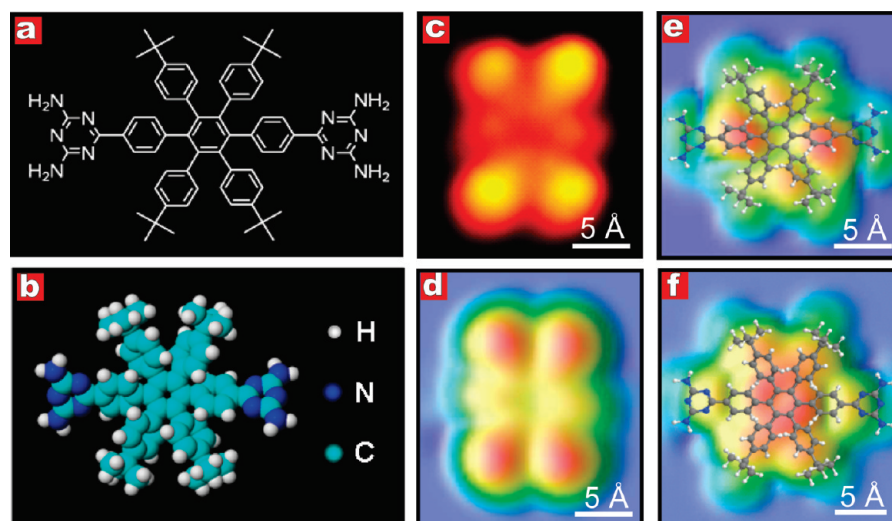
© 2010 American Chemical Society

Figure 1. (a) Chemical structure of the Lander-DAT molecule ($C_{64}H_{68}N_{10}$). (b) Corresponding space-filling model, where carbon, hydrogen and nitrogen atoms are represented in cyan, white and blue, respectively. (c) A high-resolution STM image of a single Lander-DAT molecule on a Au(111) surface (I_t = 0.32 nA, V_t = 1487 mV). (d) EHMO-ESQC calculated image of Lander-DAT on Au(111) under the same tunneling conditions as those used for the STM image in (c). (e) EHMO-ESQC calculated image of Lander-DAT at a positive bias voltage outside of the HOMO−LUMO gap, showing a weak contrast centered on the NH_2 moiety. (f) EHMO-ESQC calculated image of Lander-DAT corresponding to a resonance close to the vacuum level, giving a significant contribution on the triazine rings. For (e) and (f), a ball-and-stick model of Lander-DAT is superimposed to facilitate the attribution of the tunneling.

complementary NH···N hydrogen bonding. A related Lander molecule without DAT groups, Lander-ND, is studied for comparison. By depositing Lander-DAT on the inert, close-packed Au(111) surface under ultrahigh vacuum (UHV) conditions, we have achieved both 1-D chains as well as five distinct long-range ordered 2-D supramolecular networks and characterized these architectures using high-resolution STM. By comparing to theoretical results obtained by STM image calculations and molecular mechanics modeling, we find that the observed 1-D and 2-D structures can be rationalized through two types of intermolecular hydrogen bonding coupling motifs. Most interestingly, these coupling motifs involve pronounced 3-D optimization: The conformational flexibility allowed by the 3-D structure of the Lander-DAT molecule enables the functional DAT groups to rotate and optimize the intermolecular hydrogen bonding configurations in a way that would not have been possible in purely planar 2-D assembly. By demonstrating the first examples for the growth of extended, complex, hydrogen-bonded supramolecular surface assemblies of Lander molecules, we provide an important step toward expanding bottom-up supramolecular synthesis on 2-D substrates toward more spatial 3-D assembly.

RESULTS AND DISCUSSION

STM Imaging of Individual Lander-DAT Molecules on Au(111). The chemical structure and a space-filling model of Lander-DAT (1,4-bis(4-(2,4-diaminotriazine)phenyl)-2,3,5,6-tetrakis(4-*tert*-butylphenyl)benzene) is shown in Figure 1a,b. The compound consists of a hexaphenyl benzene (HPB) core with four *tert*-butyl groups as

spacer legs and two diamino-triazine functional groups on opposite sides to enable the intermolecular hydrogen bonding interaction. Figure 1c presents a high-resolution STM image of a single Lander-DAT molecule adsorbed on a Au(111) surface. The four bright lobes distributed in a rectangular shape (11.6 Å × 6.7 Å) are attributed to the four *tert*-butyl legs.[24,27,32] The subprotrusions in the center, which have a smaller apparent brightness, are attributed to the hexa-phenyl rings, similar to that observed earlier from a hexa-*tert*-butyl-hexa-phenyl-benzene (HB-HPB) molecule.[33] Surprisingly, however, there is no contrast in the STM image appearing to originate from the two peripheral DAT moieties.

To confirm this image interpretation and elucidate why the DAT moieties are not visible in the STM image, theoretical calculations were performed. First, molecular mechanics calculations were used to establish the conformation of an individual Lander-DAT molecule on the surface. The bulky *tert*-butyl spacer groups raise the central aromatic part of the Lander-DAT molecule to an adsorption height of 4.5 Å; the two DAT groups are not parallel to the surface plane but rotated by an angle of about 30°. Thus, the closest and the furthest nitrogen atoms in the amino-groups are of 3.1 Å and 5.2 Å above the surface plane respectively. Employing this optimized Lander-DAT adsorption conformation, a calculated STM image was obtained using the EHMO-ESQC code under the same tunneling conditions as those used in the experiment, where the bias voltage is lower than the highest occupied molecular orbital (HOMO)-lowest unoccupied molecular orbital (LUMO) gap of the molecule. The calculated result, displayed in Figure 1d,

shows that the contribution of the peripheral DAT groups to the tunneling is indeed negligible, rendering them invisible in the STM image, while the four legs are highly transparent to the tunneling electrons, leading to a predominant contribution to tunnelling and an appearance as bright protrusions. This is consistent with the experimental result.

In the case of nonfunctionalized Lander-type molecules, such as single Lander (SL, $C_{90}H_{98}$)[24,27] and violet Lander (VL, $C_{108}H_{104}$),[32] it was observed earlier that when the applied bias voltage is much smaller than the HOMO−LUMO gap of approximatively 4 eV, only the four legs are STM imaged, while the central board is not resolved. This is because the di-*tert*-butyl-phenyl spacer-leg groups are electronically interacting with the metal surface, while the central polyaromatic board is decoupled from the metal surface because of the lifting induced by the legs. As a consequence, the electronic tunnel resonance corresponding to the molecular orbitals with a large weight on the legs are broader in energy than the π and π* resonances of the central board. In the Lander HOMO−LUMO gap, the electronic transparency of the molecule is therefore controlled by the broad tails of the electronic resonance coming from the leg states. The same explanation applies to the case of Lander-DAT. To further understand why the DAT groups are not STM imaged at low bias voltage, we have also performed a molecular orbital analysis of the Lander-DAT molecule alone to track where the DAT molecular orbitals (MOs) are mainly located in energy. The analysis was performed using the Mopac (2007) method.[34] The MOs of the diamino (NH_2) moieties are electronically coupled to the DAT σ skeleton. Therefore, their contributions to the tunnelling will be outside of the range of the π MOs used in the experiments and located in the HOMO-3 to LUMO+3 energy range. The nitrogen lone pairs of the diamino are conjugated with the π MO of a triazine ring. This conjugation is only visible on the HOMO-3 and LUMO+2, which are, respectively, 2 to 3 eV away from the Fermi energy, thus, far from the used STM bias voltage range.

To explore under what conditions one might expect to obtain an STM image contrast from the DAT groups, the simulated images shown in Figure 1e,f were calculated at different given bias voltages. Ball-and-stick models of Lander-DAT are superimposed to show the corresponding part of the molecule. The calculated STM image presented in Figure 1e was obtained at the LUMO resonance energy, showing that at a positive bias voltage outside of the HOMO−LUMO gap, the first resonance will deliver a weak contrast centered on the NH_2 moiety of the DAT group. This is due to the nonplanar conformation of the diamino triazine groups which results in one of the NH_2 groups pointing up relative to the surface, reinforcing the electronic coupling with the tip and compensating for the low weight of the NH_2 MO at this energy. The first π* Lander-DAT MO with a

significant contribution on the triazine rings is located further away in energy and corresponds to LUMO+4. A constant-current STM image calculated for an energy corresponding exactly to this LUMO+4 resonance (as if a dI/dV STM image was experimentally recorded) is presented in Figure 1f, showing indeed a contrast coinciding with the position of the DAT groups in the overlaid molecular model. However, this resonance is not experimentally accessible because it is too close to the vacuum level. Nevertheless, in the experiments, it is possible under particular tip conditions to capture in the STM images certain features which can be associated to the DAT groups (see Figure 6) .

Modeling of Hydrogen-Bonded Coupling Motifs for Lander-DAT Molecules. Two possible arrangements of Lander-DAT molecules, allowing for intermolecular hydrogen bonding, may be anticipated *a priori* based on the chemical structure of the DAT functional groups; either a "Sideways" arrangement as shown in Figure 2a or a "Head-on" arrangement as shown in Figure 2b. In both cases, double N−H···N hydrogen bonds are formed between coplanar DAT moieties on adjacent molecules, similar to what have been observed previously for 2-D hydrogen-bonded surface networks of melamine molecules[35−38] and other molecules with DAT functional groups.[14]

In the bulk and gas phases, the melamine molecule itself adopts a nonplanar configuration,[39] and recent *ab initio* density functional theory calculations have demonstrated a nonplanar configuration of melamine dimers to be energetically favorable compared to a planar one, showing the stabilization energy of nonplanar configuration is slightly higher than that of the planar one (0.24 *vs* 0.22 eV per hydrogen bond).[38] Because the DAT moieties of Lander-DAT have been elevated from the surface by the bulky *tert*-butyl groups and are further σ-bonded to the phenyl rings of the central molecular board, one may anticipate a high degree of conformational flexibility for the DAT groups. This suggests that the situation for hydrogen bonding interaction between Lander-DAT molecules may be intermediate between that found in surface networks formed from planar molecules adsorbed on surfaces in flat configuration, as previously studied in many instances, and the bulk/gas phase situations. We therefore used MM4 molecular mechanics calculations to explore if the two displayed interaction motifs could be optimized using the 3-D conformational freedom of the adsorbed Lander-DAT molecules. The resulting minimum-energy situation obtained after relaxation of the "Sideways" coupling motif is displayed in Figure 2c. As indicated by dashed yellow lines in the enlarged section shown in Figure 2e, double hydrogen bonding is established in which the N−H···N bond lengths are 2.89 Å, and the N−H···N angle is 146°. In this 3-D optimized configuration, the two DAT groups are spatially rotated so that they are not coplanar but have an angle between them
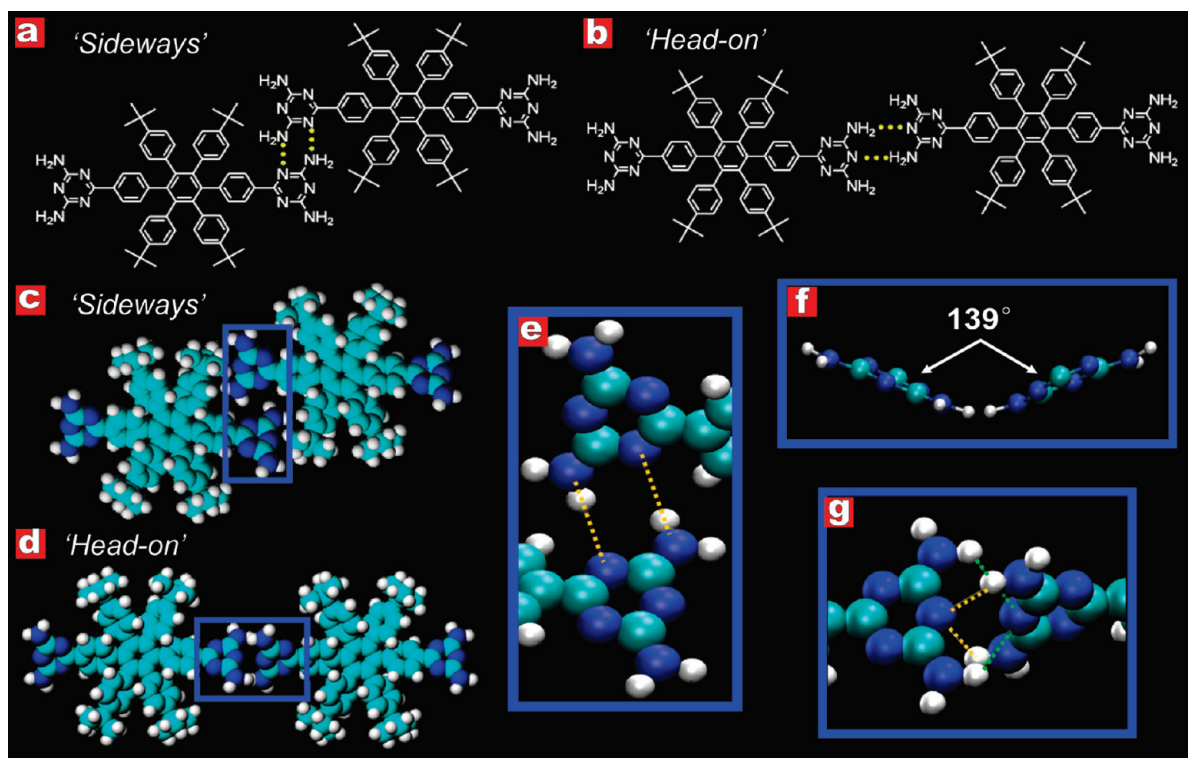
Figure 2. Anticipated and calculated arrangements of Lander-DAT dimers. (a) Anticipated "Sideways" and (b) "Head-on" coupling with double N—H···N hydrogen bonds marked by yellow dashed lines. (c) Calculated "Sideways" and (d) "Head-on" coupling arrangements obtained by full relaxation using MM4 calculations. (e) Top-view of the indicated interaction motif in the calculated "Sideways" coupling, where double N—H···N hydrogen bonds between the adjacent nonplanar DAT groups are marked by yellow dashed lines. (f) Side-view of the calculated "Sideways" coupling, showing the rotation of the neighboring DAT groups. (g) Top-view of the indicated interaction motif in the calculated "Head-on" coupling, where the rotation of the adjacent DAT groups is clearly noticeable and the two pairs of N—H···N hydrogen bonds are marked by dashed yellow and green lines, respectively.

of approximately 139° as shown in Figure 2f. The 3-D rotation effect is even more pronounced for the "Head-on" coupling where the arrangement with coplanar DAT groups, as shown in Figure 2b, did not represent a stable situation in the calculations for adsorbed molecules. Instead, the two DAT groups rotate as shown in Figure 2d to optimize the intermolecular interaction and the two Lander-DAT molecules shift laterally compared to that shown in Figure 2b so their arrangement becomes nearly coaxial. The interacting DAT groups form an angle of 75° with respect to each other, thereby allowing for the formation of four N—H···N hydrogen bonds with the two azine N atoms forming bonds to two NH groups each as indicated in Figure 2g by dashed yellow and green lines. The average N—H···N bond length and angle are 2.92 Å and 121°, respectively. The total interaction energy for the "Sideways" configuration was calculated by the MM4 modeling to be 0.682 eV, of which hydrogen bonding contributes 0.486 eV (0.243 eV per hydrogen bond) and vdW interactions 0.196 eV. For the "Head-on" dimer coupling, the corresponding energy is 0.821 eV, including a contribution from hydrogen bonding of 0.729 eV (0.182 eV per hydrogen bond) and from vdW interactions of 0.092 eV. Our results are consistent with earlier calculations for melamine dimers,[35,40,41] where a stabilization energy of

0.24 eV per hydrogen bond and a N—H···N bond length in the range of 2.8—3.0 Å were found.

If the two described coupling motifs are extended to lines by joining additional molecules in head-to-tail fashion, it will result in distinct arrangements on the surface. For the "Sideways" coupling motif the molecular axis (*i.e.*, the line across the centers of the two DAT end groups) will be rotated by 19° away from the orientation of the stripe as defined by a line through the molecular centers and the calculated periodicity along this line is 17.0 Å. For the "Head-on" case the periodicity (*i.e.*, intermolecular distance) along the molecular line is 20.1 Å and the molecular axis is rotated by just 5° off the direction of the molecular line. The "Sideways" coupling is thus more condensed than the "Head-on" case with a shorter periodicity (17.0 *vs* 20.1 Å) and a larger rotation angle of each molecule relative to the stripe axis (19 *vs* 5°).

STM Results and Models for Extended Adsorption Structures. Turning to the STM experiments, we first describe results obtained by depositing Lander-DAT at low coverage. Here 1-D chains of Lander-DAT molecules form both at the step edges and on the terraces, as shown by the STM images displayed in Figure 3a,b, respectively. The chains aligned by step edges are long-range ordered and can extend over hundreds of nanometers. This decoration effect may partly originate from charge redistribution at the
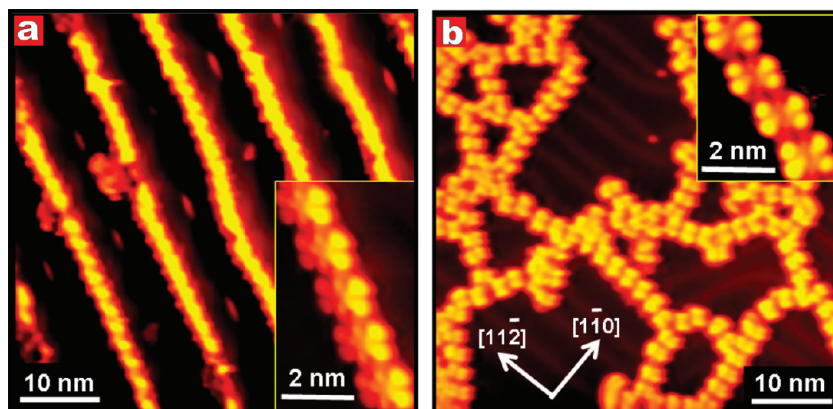
Figure 3. (a) STM image of 1-D Lander-DAT chains at step edges of Au(111) (I_t = 0.70 nA, V_t = 1250 mV) with a high-resolution image shown in the inset (I_t = 0.48 nA, V_t = 1487 mV). (b) STM image of 1-D structures of Lander-DAT on terraces of Au(111) (I_t = 0.52 nA, V_t = 1250 mV) with a close-up view of a 1-D chain segment shown in the inset (I_t = 0.46 nA, V_t = 1250 mV).

metallic step edges (Smoluchowski effect). A zoom-in showing such a chain at submolecular resolution is displayed in the inset of Figure 3a. The periodicity along the chain is 17.0 ± 0.5 Å and the Lander-DAT molecules are oriented such that their axis is rotated away from the direction of the chain by approximately 18°. These observations are consistent with the parameters (17.0 Å and 19°) obtained from the theoretical modeling of the "Sideways" configuration described above. Two of the four lobes corresponding to the spacer legs of each Lander-DAT have a higher brightness, suggesting that the molecules in the chain are inclined on the step edge with two legs on upper/lower terraces, respectively.[18] The chains formed on the terraces consist of shorter segments, leading to a structure without long-range order (Figure 3b. The Lander molecules in the chains typically have their axis aligned along ⟨11$\bar{2}$⟩ directions of the underlying Au(111) substrate. A high-resolution STM image (inset of Figure 3b) further shows that these chains have the same "Sideways" coupling as observed at the step edges. As seen in the main image of Figure 3b, the herringbone reconstruction of the Au(111) substrate is not disturbed by the adsorbates, implying that the molecule−substrate interaction is rather weak although it may affect the adsorption orientation of the Lander-DAT molecules.

At higher coverage, five distinct 2-D structures of Lander-DAT molecules were observed on the terraces

of the Au(111) surface. These phases will be denoted "Six-Blade Mill" ("SM"), "Four-Blade Mill" ("FM"), "Grid", "Transition", and "Close-Packed Stripe" ("Stripe" for short). The different phases are described in detail below, and their structural parameters as obtained from both experimental data and theoretical modeling are summarized in Table 1.

"SM" and "FM" Adsorption Structures. Overview and high-resolution STM images of the "SM" and "FM" phases are presented in panels a and b of Figures 4 and 5, respectively. Both phases are observed as extended islands on the Au(111) surface. The "FM" phase appears as a defect-free network, which is generally more ordered than the "SM" phase. One common feature for the two phases is that they can both be viewed as being built up from a tiling of characteristic Lander-DAT dimer motifs. These dimers are indicated in Figure 4b and Figure 5b by transparent rectangles across the centers of paired molecules, illustrating how the tiling of the dimers leads to four and six-blade mill structures.

For the "SM" phase, the dimers adopt all three symmetry equivalent orientations on the surface, marked by white, green, and blue rectangles, with an angle of 60° between one and another; while for the "FM" phase, only dimers in two orientations are involved, indicated by green and blue rectangles which are normal to each other. In both cases, the molecules are adsorbed with

TABLE 1. Comparison of Structural Parameters for the Different Phases of Lander-DAT and Lander-ND Observed on the Au(111) Surface

|	experimental results					theoretical calculations		
	length of vectors (Å)					length of vectors (Å)		
	a	b	included angle (deg)	density (molecule/nm^2)	coupling	a	b	included angle (°)
chain on terraces	17.0				sideways	17.0		
SM	36.4	36.4	60	0.523	sideways	36.5	36.5	61
FM	27.2	27.2	90	0.541	sideways	28.0	28.0	90
Grid	20.8	28.5	60	0.390	head-on	20.1	31.6	58
Tran. A	17.0	52.5	88	0.336	sideways	17.0	54.0	88
Stripe	16.5	17.0	60	0.412	sideways	17.7	17.7	55
Lander ND	12.5	15.4	85	0.521		13.2	15.9	89
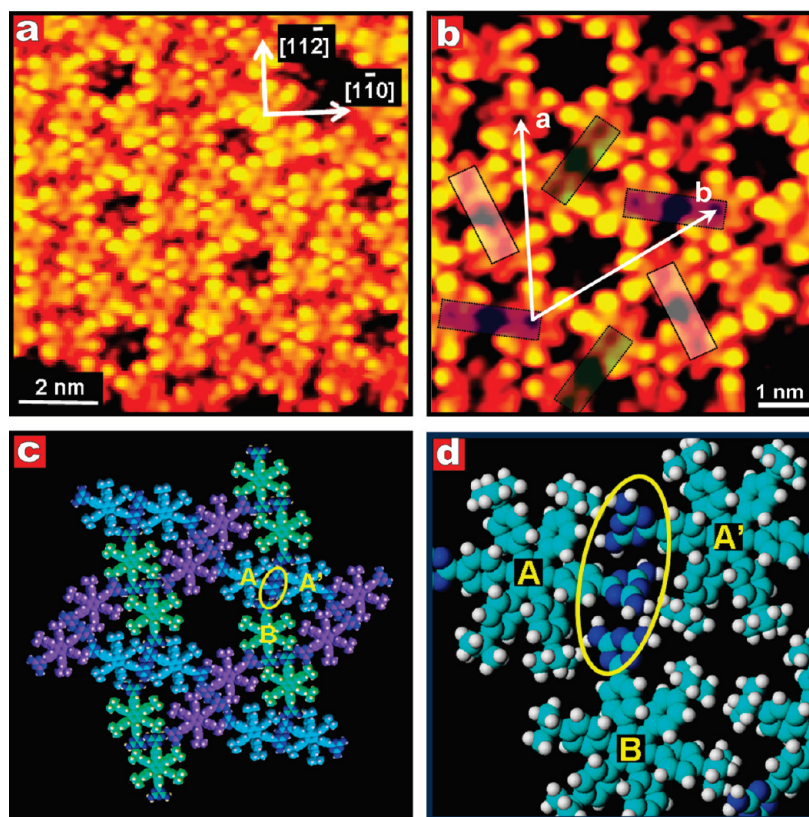
Figure 4. "Six-Blade Mill" ("SM") phase of Lander-DAT on Au(111). (a) Large-scale STM image with high-symmetry directions of the Au(111) substrate indicated (I_t = 0.23 nA, V_t = 1165 mV). (b) High-resolution STM image (I_t = 0.24 nA, V_t = 1165 mV), showing that the "SM" phase is composed of Lander-DAT dimers in three different orientations marked by the transparent rectangles in white, green, and blue, with an angle of 60° between one another. (c) Model of "SM" phase obtained by superimposing carefully scaled space-filling model of Lander-DAT onto the experimental STM images. DAT dimers in different orientations are presented in pale blue, green, and purple, respectively. (d) Section of the theoretically calculated structure for the "SM" phase centered on the node highlighted by the yellow ellipse in (c). The rotation of neighboring DAT groups for 3-D optimized intradimer and interdimer hydrogen bonding interaction is clearly visible, where the molecules marked A, A′ correspond to the dimer in pale blue and the molecule marked B corresponds to the neighboring molecule in green in (c).

their main axis along ⟨11$\bar{2}$⟩ directions of the Au(111) substrate, that is, the angle between molecules in different orientations is 60°. Notice that the indicated orientation of the dimers is different from that of the individual molecules in the dimers. As summarized in Table 1, the unit-cell vectors for the "SM" phase have lengths of $|a| = |b|$ = 36.4 ± 1.0 Å, and the included angle is 60°, giving a molecular density of 0.523 molecule per nm². The unit cell vectors for the "FM" phase have lengths of $|a| = |b|$ = 27.2 ± 1.0 Å and the included angle is 90°, giving a density of 0.541 molecule per nm².

Models for the "SM" and "FM" phases, obtained by superimposing carefully scaled space-filling models of Lander-DAT molecules onto the experimental STM images (*e.g.*, Figures 4b and 5b), are illustrated in Figure 4c and 5c, respectively. Colors are used to indicate the individual Lander-DAT dimers, and identical colors are used for dimers in identical orientations. Starting from these model configurations, molecular mechanics calculations were performed for molecules adsorbed on the unreconstructed Au(111) surface to optimize molecular orientations and conformational degrees of free-

dom with the aim to identify intermolecular interaction motifs that may drive formation of the experimentally observed structures. The unit cell parameters for the energy-minimized calculated structures, provided in Table 1, are consistent with the experimental values. Enlarged views of calculated configurations for the "SM" and "FM" phases are presented in Figures 4d and 5d, respectively, centered on the portion of the structures highlighted by yellow ellipses in Figures 4c and 5c, which constitute the most interesting interaction nodes. In Figure 4d, the molecules marked A and A′ correspond to the molecules of the dimer indicated by pale blue in Figure 4c, and the molecule marked B corresponds to the closest molecule of the neighboring dimer indicated by green color. Similarly, in Figure 5d, A, A′ and B, B′ correspond to the dimers in pale blue and green in Figure 5c, respectively. The close-up views of the calculated models in both cases display an intermolecular hydrogen bonding network optimized in three dimensions: each dimer is stabilized by double N−H···N hydrogen bonds between rotated DAT moieties arranged in a
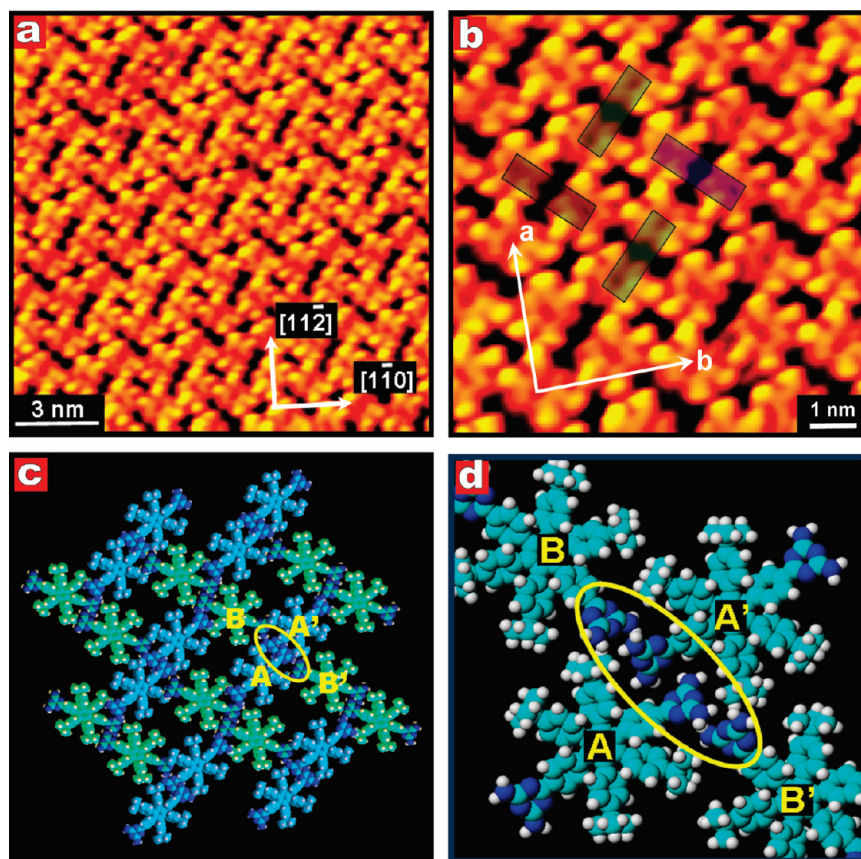
Figure 5. "Four-Blade Mill" ("FM") phase of Lander-DAT on Au(111). (a) Large-scale STM image with high-symmetry directions of the Au(111) substrate superimposed (I_t = 0.50 nA, V_t = 1250 mV). (b) High-resolution STM image (I_t = 0.47 nA, V_t = 1250 mV), showing that the "FM" phase is composed of Lander-DAT dimers in two orientations normal to each other, marked by the transparent rectangles in green and blue. (c) Model of the "FM" phase obtained by superimposing carefully scaled space-filling model of Lander-DAT onto the STM image in (b). "Sideways" coupled DAT dimers in two orientations are presented in pale blue and green, respectively. (d) Section of the theoretically calculated structure for the "FM" phase centered on the node indicated by the yellow ellipse in (c), showing the rotation of neighboring DAT groups for 3-D optimized intradimer and interdimer hydrogen bonding interaction. Molecules marked A, A′ correspond to the dimer in pale blue in (c), while molecules marked B, B′ correspond to the neighboring dimer in green.

"Sideways" coupling similar to that presented in Figure 2e. The bond lengths and interaction angles of the hydrogen bonding are similar to the situation for the single-dimer case. In addition to this intradimer interaction (see the DAT groups of molecule A and A′ in Figures 4d and 5d), the networks are further stabilized by additional interdimer double N−H···N hydrogen bonding to the DAT groups of the nearest neighboring molecules, which are not involved in the intradimer hydrogen bonding (see the DAT groups of molecule A and B in Figure 4d; the DAT groups of molecule A and B′, as well as A′ and B in Figure 5d).

"Grid" and "Stripe" Structures. Large-scale and high-resolution STM images of the "Grid" phase are depicted in Figure 6a,b, respectively. The molecules in this phase appear in two different arrangements: some (A-type) stack to form rows running along the direction indicated by transparent blue rectangles in Figure 6a; while the remaining molecules (B-type), indicated by green rectangles, interconnect these rows. The associated model is shown in Figure 6c, where the Lander-DAT molecules in the row-like structures are shown in

blue, while the molecules connecting the rows are shown in green. Both A-type and B-type molecules are aligned with their main axis along ⟨1$\bar{1}$0⟩ type directions of the Au(111) substrate, hence, the angle between them is 60°. The "Grid" phase has unit cell vectors of $|a|$ = 20.8 ± 1.0 Å and $|b|$ = 28.5 ± 1.0 Å and an included angle of 60°, yielding a density of 0.390 molecule per nm². Also, for this structure, an optimized model with structural parameters (see Table 1) consistent with the experimental values was obtained from molecular mechanics calculations. The rows formed by pairing of A-type molecules have a periodicity of 20.8 Å and the molecules are arranged with their axis rotated by less than 10° from the direction of the rows. This is in a good agreement with the "Head-on" configuration depicted in Figure 2g and clearly distinct from the arrangement and intermolecular distances observed for the 1-D chains and the "SM" and "FM" phases, which are stabilized by "Sideways" coupling. A close-up view of the calculated model is presented in Figure 6d, showing the structural details of the interaction node involving four adjacent DAT groups. The molecules marked
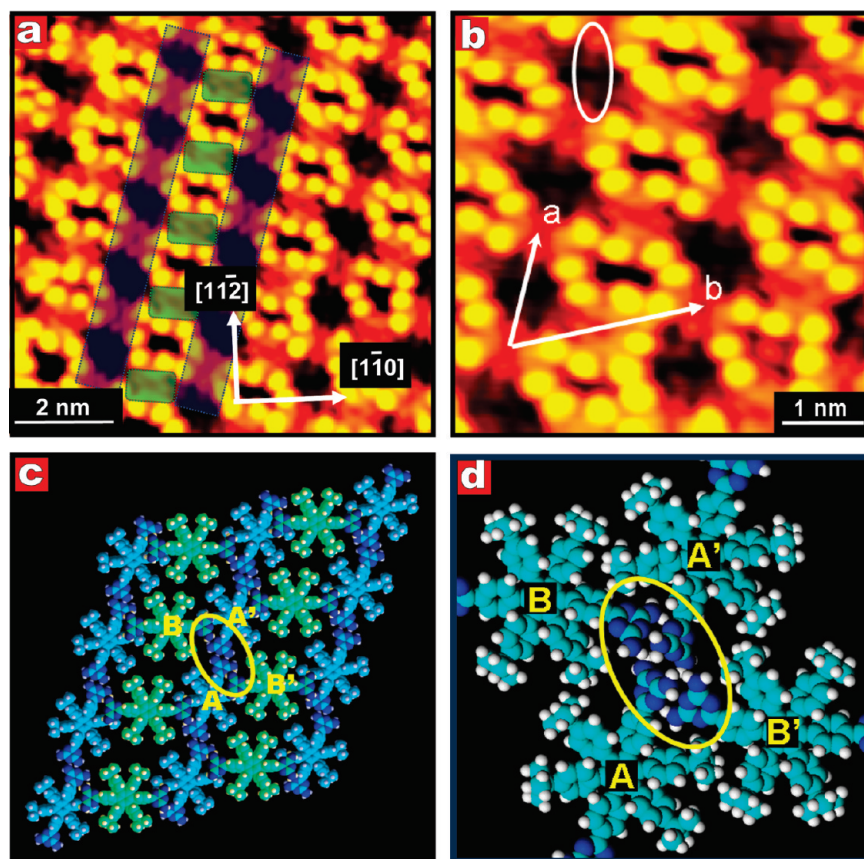
Figure 6. "Grid" phase of Lander-DAT on Au(111). (a) Large-scale STM image of the "Grid" phase with high-symmetry directions of the Au(111) substrate superimposed (I_t = 0.44 nA, V_t = 1250 mV). Row-like motifs of Lander-DAT are indicated by transparent blue rectangles while interconnecting molecules are indicated by green rectangles. **(b)** High-resolution STM image of the "Grid" phase (I_t = 0.42 nA, V_t = 1250 mV), showing molecules aligned with the main axis along $\langle 1\bar{1}0 \rangle$ type directions of the Au(111) substrate. The topmost white ellipse indicates features attributed to the DAT groups. **(c)** Model of the "Grid" phase obtained by superimposing carefully scaled space-filling model of Lander-DAT on the STM image in (b), where the Lander-DAT molecules in row-like structures are in pale blue and the connectors are in green. **(d)** Section of the theoretically calculated structure for the "Grid" phase centered on the node indicated by a yellow ellipse in (c) and showing the rotation of the DAT groups. The molecules marked A, A′ and B, B′ correspond to two "Head-on" coupled molecules in pale blue and the two connectors in green in (c), respectively.

A, A′ are indeed stabilized by double N—H⋯N hydrogen bonding in "Head-on" coupling, while the B-type molecules interconnect the rows by additional double hydrogen bonding to the DAT groups of the A-type molecules.

We finally remark that in high-resolution STM images of the "Grid" structure, obtained under special tip conditions, the molecules in the "Head-on" row arrangement displays features (indicated by a white ellipse Figure 6b) that can be directly attributed to tunneling associated with the DAT groups.

Figure 7a,b displays STM images of the "Close-Packed Stripe" phase, which is observed as extended, well-ordered islands. The unit cell of this phase has dimensions of $|a|$ = 16.5 ± 0.5 Å, $|b|$ = 17.0 ± 0.5 Å, and an included angle of 60°, yielding a density of 0.412 molecule per nm². The Lander-DAT molecules in this case are all in an identical arrangement, typically aligned along $\langle 11\bar{2} \rangle$ directions of the Au(111) substrate. The structure is consequently observed in three rotational domains on the surface. A model based on

the STM images is presented in Figure 7c, while Figure 7d shows a close-up view of the corresponding optimized structural model resulting from theoretical calculations. Each stripe is stabilized by double N—H⋯N hydrogen bonding between adjacent molecules. The periodicity along the **b** direction of the unit cell (17.0 Å) is consistent with that for "Sideways" coupling depicted in Figure 2c. These parallel stripes are close-packed side by side, most likely stabilized by vdW forces. In contrast to the structures described above, there is no additional hydrogen bonding from neighboring molecules involved in the interaction nodes.

"Transition" Phases. Figure 8 shows results for the "Transition" phase, which is intermediate in structure between the "Grid" and the "Stripe" phases. Two types of "Transition" structures are observed. Figure 8a,b shows large-scale and high-resolution STM images of one of them ("Tran. A"). Its corresponding model obtained by superimposing carefully scaled space-filling models of Lander-DAT on the experimental STM images is provided in Figure 8c. The "Tran. A" phase has a unit
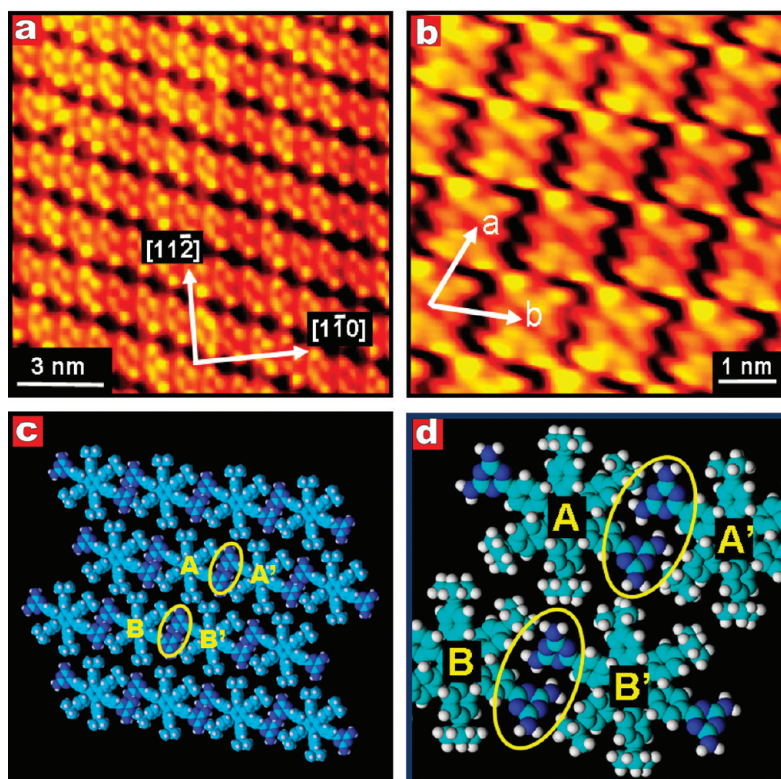
Figure 7. "Stripe" phase of Lander-DAT on Au(111). (a) Large-scale STM image of the "Stripe" phase ($I_t = 0.48$ nA, $V_t = 1250$ mV), showing close-packed parallel stripes of Lander-DAT. (b) High-resolution STM image of the "Stripe" phase ($I_t = 0.48$ nA, $V_t = 1250$ mV). (c) Structural model obtained by superimposing carefully scaled space-filling model of Lander-DAT on the experimental STM images. (d) Section of the theoretically calculated structure for the 'Stripe' phase centered on the node indicated by yellow ellipses in (c), where double N−H···N hydrogen bonding occurs between the molecules marked A, A′ and B, B′ as they undergo "Sideways" coupling.

cell with vectors of $|a| = 17.0 \pm 0.5$ Å and $|b| = 52.5 \pm 2.0$ Å and an included angle of 88°, yielding a density of 0.336 molecule per nm². Similar to the "Grid" phase, the "Tran. A" phase is composed of molecules in two orientations: A-type stacked into rows and B-type connected sideways to these rows (see Figure 8c). Both A- and B-type molecules are aligned along $\langle 1\bar{1}0 \rangle$ type directions of the Au(111) surface. The structure can be rationalized from "B-A-B" motifs consisting of one row of A-type molecules surrounded by rows of B-type molecules. These motifs repeat to form the extended structure. The periodicity and orientation of the A-type molecules in the "Tran. A" phase suggests that they adopt the "Sideways" arrangement similar to that observed for the "Stripe" phase, but different from the "Grid" phase, where the rows were based on the less close-packed "Head-on" coupling, As a consequence, the spacing between neighboring B-type molecules along the rows is shorter than in the case of the "Grid" phase. A closely related "Transition" phase ("Tran. B") is shown in Figure 8d, presenting an "A-B-A" sandwich structure where two rows of A-type molecules joined by "Sideways" coupling are held together by B-type connectors. A model based on the STM images is depicted in Figure 8e.

The MM4 calculations also in this case provide relaxed models with structural parameters in good agree-ment with the experimental results (See Table 1). An enlarged view of the calculated model representative for both the "Tran. A" and the "Tran. B" phases is presented in Figure 8f. In the region highlighted by the yellow ellipse, the DAT groups of neighboring A and A′ molecules are rotated to join in a "Sideways" coupling motif involving double hydrogen bonding. The B-type molecules connect sideways to these interaction motifs by additional double hydrogen bonding. For the "Tran. A" domain in Figure 8a,b, further hydrogen bonding occurs between the DAT moieties on the B-type molecules of two neighboring B-A-B motifs and also, in this case, by "Sideways" coupling.

Lander-ND Adsorption Structure. To further elucidate the role played by the functional DAT moieties in the molecular self-assembly described above, we synthesized and investigated a related compound, Lander-ND ($C_{58}H_{62}$) for comparison. Lander-ND has the same structure as Lander-DAT except that the DAT groups are missing as shown in Figure 9(a) and 9(b). A high-resolution STM image of an individual Lander-ND molecule adsorbed on the Au(111) surface is displayed in Figure 9(c), showing a morphology similar to that observed for Lander-DAT (compare to Figure 1). A calculated STM image of a fully relaxed Lander-ND molecule on the surface was obtained using the ESQC approach and is shown in Figure 9(d). There is good quantitative
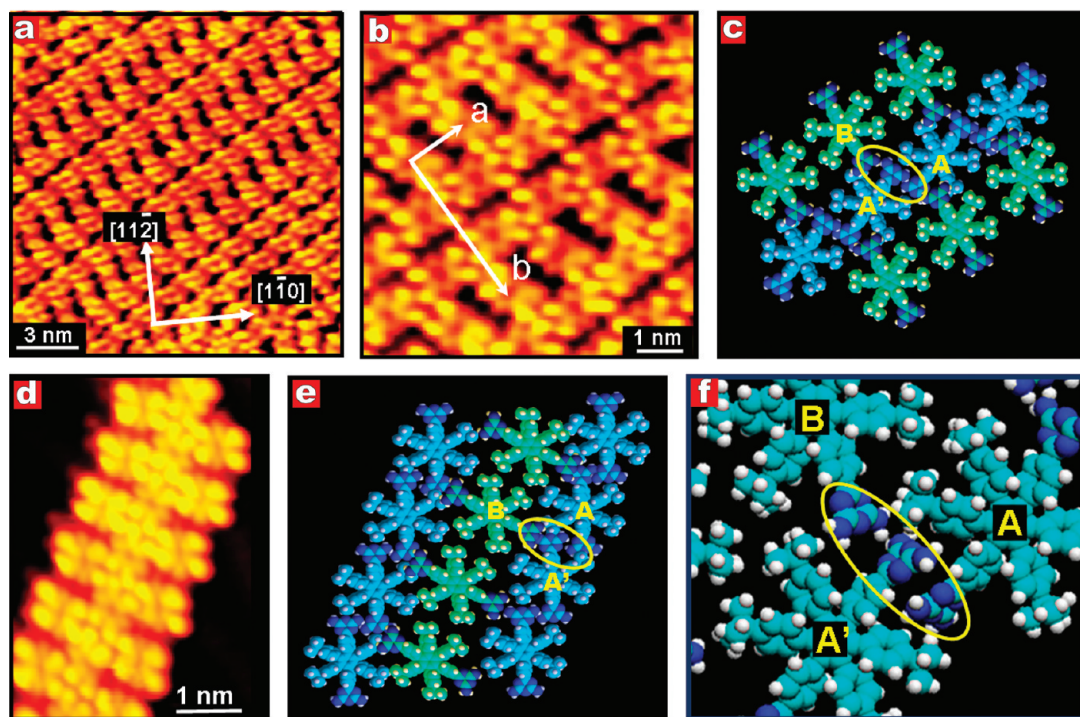
Figure 8. "Transition" phase of Lander-DAT on Au(111). (a) Large-scale STM image of the "Tran. A" phase ($I_t = 0.40$ nA, $V_t = 1250$ mV). The orientations of Au(111) substrate are pointed out. (b) High-resolution STM image of the "Tran. A" phase ($I_t = 0.28$ nA, $V_t = 1250$ mV). (c) Structural model obtained by superimposing carefully scaled space-filling model of Lander-DAT onto the experimental STM images. (d) STM image of the "Tran. B" phase ($I_t = 0.39$ nA, $V_t = 1250$ mV). (e) Structural model corresponding to the image in (d). (e) Section of the theoretically calculated structure for the "Transition" phase centered on the node indicated by a yellow ellipse in both (c) and (e), showing the rotation of neighboring DAT groups for 3-D optimized hydrogen bonding interaction. The molecules marked A, A′ correspond to the "Sideways" coupled A-type molecules in pale blue while the molecule marked B corresponds to the neighboring B-type molecule shown in green in both (c) and (e).

agreement with the experimental results. Similarly to the case for Lander-DAT, we attribute the four bright lobes in a rectangular shape (11.0 Å × 6.5 Å) to the four *tert*-butyl groups, and the subprotrusions in the center to the hexa-phenyl rings.

We only observed a single adsorption structure for Lander-ND on the Au(111) surface, namely, a close-packed row structure, for which an STM image and an adsorption model are shown in Figure 9e,f, respectively. The unit cell for this structure has the dimensions of

$|a| = 12.5 \pm 0.5$ Å and $|b| = 15.4 \pm 0.5$ Å, with an included angle of 85°, yielding a density of 0.521 molecule per nm². In this structure, the Lander-ND molecules also adopt an orientation with their axis (between the unsubstituted phenyl groups) along $\langle 11\bar{2} \rangle$ directions of the Au(111) substrate. The Lander-ND structure resembles the "Stripe" phase of Lander-DAT, but has a higher molecular density and a shorter periodicity along the rows (12.5 *vs* 17.0 Å) and a smaller rotation angle of each molecule relative to the stripe axis (15 *vs*
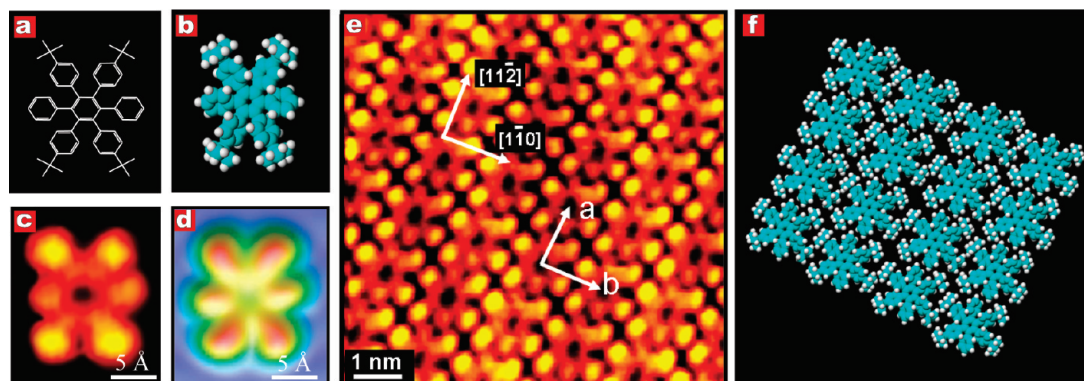

Figure 9. (a) Chemical structure of Lander-ND molecule ($C_{58}H_{62}$). (b) Corresponding space-filling model, where carbon and hydrogen are represented in cyan and white, respectively. (c) High-resolution STM image of a single Lander-ND on Au(111) ($I_t = 0.31$ nA, $V_t = 1250$ mV). (d) EHMO-ESQC calculated image of Lander-ND on Au(111) under the same tunneling conditions as those used for the STM image in (c). (e) STM image of closed-packed Lander-ND molecules on Au(111) ($I_t = 0.31$ nA, $V_t = 1250$ mV). (f) Calculated model of close-packed Lander-ND molecules after full relaxation.

19°). An optimized structural model was obtained from MM4 calculations, which is consistent with the experimental structural parameters, as shown in Table 1. We suggest that within the Lander-ND rows, the molecules are stabilized by vdW interaction.

Comparison of Adsorption Structures. Thermal evaporation of large and complex organic compounds, such as the 3-D Lander molecules studied here, involves a risk of thermal decomposition if the intermolecular cohesive strength in the molecular source material exceeds the intramolecular binding energy. Therefore, the absence of a clear signature in the STM images of the functional DAT groups could in principle cause concern that these groups were lost due to thermal fragmentation during sublimation of the Lander-DAT molecules onto the surface. However, due to the electronic structure of the Lander-DAT molecules, an STM contrast originating from the DAT group is in fact not to be expected under the experimentally applied STM imaging conditions, as demonstrated from the presented calculations of STM images. Furthermore, the striking contrast between the richness of structures resulting from deposition of Lander-DAT and the singular structure observed in the control experiments with Lander-ND, which has a chemical structure similar to that expected for Lander-DAT if the DAT groups were lost, provides additional support that the DAT functional moieties are indeed retained and guide the assembly of the observed adsorption structures.

Despite the great variation of observed structures for Lander-DAT on the Au(111) surface, certain unifying motifs are clearly emerging from the analysis presented above. In particular, the characteristic dimer motifs observed in the "SM" and "FM" structures involve the same relative molecular arrangements as found in the isolated molecular rows, observed on the terraces and at step edges at low coverage, and in the row motifs observed to be embedded in the "Stripe" and "Transition" phases. Interestingly, it was not possible to account quantitatively for most of the observed structures by simple overlays of rigid molecular models involving DAT groups parallel to the surface plane. A detailed analysis of several of the presented crude structures used as input to the theoretical modeling instead reveal steric crowding and collisions of DAT groups on neighboring molecules. However, by invoking and optimizing the conformational degrees of freedom for the DAT groups, as was done in the molecular mechanics calculations, it was indeed possible in all cases to obtain convincing structural models that were in good quantitative agreement with the experimentally observed structures and detailed unit cell parameters. A thorough analysis of the theoretically calculated models shows that both 3-D optimized hydrogen bonding interaction motifs, that is, "Sideways" and "Head-on" couplings, participate in the structures formed. The "Sideways" interaction motif is most common and oc-

curs for the isolated rows (Figure 3), the "SM" (Figure 4) and "FM" (Figure 5) phases, as well as for the "Stripe" (Figure 7) and "Transition" (Figure 8) phases. The "Head-on" motif, involving a longer intermolecular distance, is only identified in the "Grid" structure (Figure 6). It is somewhat surprising that the "Sideways" interaction motif is observed most often because the dimer in "Sideways" coupling was found from the theoretical modeling to be less strongly bound compared to the dimer in "Head-on" arrangement. However, in all of the experimentally observed structures involving dimerization, except for the "Stripe" phase, the calculated models suggest that the interaction nodes involve additional hydrogen bonding interactions to adjacent molecules, which are not taken into account in the reported calculations for the pure dimer structures of Figure 2.

Besides intermolecular hydrogen bonding, the interaction between Lander-DAT and the Au(111) substrate also affects the adsorption of Lander-DAT molecule. The molecular axis of the Lander-DAT molecules orients along $\langle 11\bar{2} \rangle$ directions of the Au(111) substrate for the isolated rows observed on terraces as well as for the "SM", "FM", and "Stripe" phases, and along $\langle 1\bar{1}0 \rangle$-type directions for the "Grid" and "Tran. A" phases. Therefore, the self-assembly most likely results from an interplay between the intermolecular interaction and the molecule−substrate interaction. Considering the singular structure obtained for Lander-ND, it is evident that the DAT group and associated functionality for intermolecular hydrogen bonding is the main factor driving the variety of distinct Lander-DAT structures on Au(111).

CONCLUSIONS AND OUTLOOK

In summary, we have investigated the self-assembly of a specially designed 3-D Lander molecule, Lander-DAT, on the Au(111) surface by a combination of *in situ* STM imaging and theoretical modeling of molecular structures and calculated STM images. We find that the diamino-triazine functional groups indeed guide the self-assembly of both 1-D and a range of distinct 2-D supramolecular nanostructures. A crucial element in accounting for the observed molecular Lander-DAT structures is the conformational flexibility of the functional DAT groups, allowed by the pronounced 3-D structure of the Lander molecules with bulky leg groups. Two molecular interaction motifs are discussed, which could not be realized in self-assembly utilizing planar compounds with similar functionality, but adsorbed directly on the surface,[14,35−38] because they involve 3-D optimization of the intermolecular hydrogen bonding.

The experimental results presented here constitute the first examples of long-range, well-ordered 2-D organic architectures built up from Lander molecules

through the use of intermolecular hydrogen bonding interactions. Because the interactions responsible for the structures are intrinsic to the molecules themselves and are not provided by surface templating effects, as studied before,[28–30,32] it may be possible to transfer the structural synthesis to other substrates such as insulators or thin insulating films more relevant for studying, for example, the electronic properties of the molecular assemblies. A particularly interesting direction for further studies is provided by the remarkable property of Lander-type molecules to act as molecular molds by trapping and assembling metal atoms into a well-defined metallic nanostructure in the cavity underneath the aromatic board.[24–27] The 1-D and 2-D patterns of Lander-DAT molecules described here may be envisioned to act as extended molds for the growth of complex metallic nanostructures, such as metallic wires, networks, or arrays of nanodots of interest, with respect to forming and connecting to molecular electronic circuitry and quantum devices.

METHODS

The synthesis of Lander-DAT and Lander-ND has been described elsewhere.[42,43] The present experiments were conducted in a UHV chamber (base pressure $\sim 10^{-10}$ Torr) equipped with a variable-temperature Aarhus STM.[44] The Au(111) single-crystal sample was cleaned by repeated cycles of 1.5 keV Ar^+ bombardment and annealing of 850 K for 15 min. Molecules were deposited by thermal sublimation from evaporators held at ~ 530 K for Lander-DAT and at ~ 465 K for Lander-ND, respectively. The Lander-DAT and Lander-ND molecules were thoroughly degassed prior to deposition. The molecules were deposited onto a Au(111) sample held at either 160−200 K or room temperature (260−300 K). In both cases, annealing of the Au(111) sample at 400 K was performed for 10 min after molecular deposition to allow an approach to thermodynamic equilibrium. All STM data presented here were collected in the constant current mode in a temperature range of 110−160 K to stabilize the molecular structures on the surface. We did not observe a clear correlation between the deposition parameters and the formation of the different phases discussed, in part because the statistical sampling was insufficient to allow quantitative comparison of their relative occurrence. The STM scanner was calibrated by atomically resolved images of the Au(111) surface. With this procedure a statistical spread of ~ 0.5 Å is obtained on the dimension of Lander-DAT molecules observed in different images/phases. Theoretical calculations of STM images were performed using the extended Hückel molecular orbital-elastic-scattering quantum chemistry (EHMO-ESQC) technique.[45] Molecular surface structures were modeled using the force-field method, as developed in the MM4(2003) code,[46] which is optimized for treating vdW interactions between molecules and hydrogen bonding. We adopted the same MM4 parametrization as in recent ASED+ calculations describing the physisorption of large molecules on Au(111).[47,48] In the present calculations, molecules were initially placed on the unreconstructed Au(111) surface at positions that represent a compromise between the optimum adsorption sites established for individual molecules and the approximate structures for dimers and extended structures as derived from the STM images. These configurations were subsequently relaxed/optimized with respect to lateral position and orientation of the molecules on the surface, as well as molecular internal degrees of freedom, such as rotations of molecular bonds, while the surface atoms were kept fixed.

REFERENCES AND NOTES

1. Joachim, C.; Gimzewski, J. K.; Aviram, A. Electronics Using Hybrid-Molecular and Mono-Molecular Devices. *Nature* **2000**, *408*, 541–548.

2. Browne, W. R.; Feringa, B. L. Making Molecular Machines Work. *Nat. Nanotechnol.* **2006**, *1*, 25–35.

3. Barth, J. V.; Weckesser, J.; Cai, C.; Günter, P.; Bürgi, L.; Jeandupeux, O.; Kern, K. Building Supramolecular Nanostructures at Surfaces by Hydrogen Bonding. *Angew. Chem., Int. Ed.* **2000**, *39*, 1230–1234.

4. Kühnle, A.; Molina, L. M.; Linderoth, T. R.; Hammer, B.; Besenbacher, F. Growth of Unidirectional Molecular Rows of Cysteine on Au(110)-(1×2) Driven by Adsorbate-Induced Surface Rearrangements. *Phys. Rev. Lett.* **2004**, *93*, 086101.

5. Böhringer, M.; Morgenstern, K.; Schneider, W.-D.; Berndt, R.; Mauri, F.; De Vita, A.; Car, R. Two-Dimensional Self-Assembly of Supramolecular Clusters and Chains. *Phys. Rev. Lett.* **1999**, *83*, 324–327.

6. Cañas-Ventura, M. E.; Xiao, W.; Wasserfallen, D.; Müllen, K.; Brune, H.; Barth, J. V.; Fasel, R. Self-Assembly of Periodic Bicomponent Wires and Ribbons. *Angew. Chem., Int. Ed.* **2007**, *46*, 1814–1818.

7. Dmitriev, A.; Lin, N.; Weckesser, J.; Barth, J. V.; Kern, K. Supramolecular Assemblies of Trimesic Acid on a Cu(100) Surface. *J. Phys. Chem. B* **2002**, *106*, 6907–6912.

8. Griessl, S.; Lackinger, M.; Edelwirth, M.; Hietschold, M.; Heckl, W. M. Self-Assembled Two-Dimensional Molecular Host-Guest Architectures From Trimesic Acid. *Single Mol.* **2002**, *3*, 25–31.

9. Stepanow, S.; Lin, N.; Vidal, F.; Landa, A.; Ruben, M.; Barth, J. V.; Kern, K. Programming Supramolecular Assembly and Chirality in Two-Dimensional Dicarboxylate Networks on a Cu(100) Surface. *Nano Lett.* **2005**, *5*, 901–904.

10. Theobald, J. A.; Oxtoby, N. S.; Phillips, M. A.; Champness, N. R.; Beton, P. H. Controlling Molecular Deposition and Layer Structure With Supramolecular Surface Assemblies. *Nature* **2003**, *424*, 1029–1031.

11. Keeling, D. L.; Oxtoby, N. S.; Wilson, C. M.; Humphry, J. N.; Champness, R; Beton, P. H. Assembly and Processing of Hydrogen Bond Induced Supramolecular Nanostructures. *Nano Lett.* **2003**, *3*, 9–12.

12. Hoeben, F. J. M.; Zhang, J.; Lee, C. C.; Pouderoijen, M. J.; Wolffs, M.; Wurthner, F.; Schenning, A. P. H. H.; Meijer, E. W.; De Feyter, S. Visualization of Various Supramolecular Assemblies of Oligo(*para*-phenylenevinylene)-Melamine and Perylene Bisimide. *Chem.—Eur. J.* **2008**, *14*, 8579–8589.

13. Surin, M.; Janssen, P. G. A.; Lazzaroni, R.; Leclere, P.; Meijer, E. W.; Schenning, A. P. H. J. Supramolecular Organization of ssDNA-Templated pi-Conjugated Oligomers *via* Hydrogen Bonding. *Adv. Mater.* **2009**, *21*, 1126–1130.

14. Miura, A.; Johkheijm, P.; De Feyter, S.; Schenning, A. P. H. J.; Meijer, E. W.; De Schryver, F. C. 2D Self-Assembly of Oligo(*p*-phenylene vinylene) Derivatives: From Dimers to Chiral Rosettes. *Small* **2005**, *1*, 131–137.

15. Gesquiere, A.; Jonkheijm, P.; Hoeben, F. J. M.; Schenning, A. P. H. J.; De Feyter, S.; De Schryver, F. C.; Meijer, E. W. 2D-Structures of Quadruple Hydrogen Bonded Oligo(*p*-phenylenevinylene)s on Graphite: Self-Assembly Behavior and Expression of Chirality. *Nano Lett.* **2004**, *4*, 1175–1179.

16. EichhorstGerner, K.; Stabel, A.; Moessner, G.; Declerq, D.;

Valiyaveettil, S.; Enkelmann, V.; Mullen, K.; Rabe, J. P. Self-Assembly of a Two-Component Hydrogen-Bonded Network: Comparison of the Two-Dimensional Structure Observed by Scanning Tunneling Microscopy and the Three-Dimensional Crystal Lattice. *Angew. Chem., Int. Ed.* **1996**, *35*, 1492–1495.

17. Otero, R.; Hümmelink, F.; Sato, F.; Legoas, S. B.; Thostrup, P.; Lægsgaard, E.; Stensgaard, I.; Galvão, D. S.; Besenbacher, F. Lock-and-Key Effect in the Surface Diffusion of Large Organic Molecules Probed by STM. *Nat. Mater.* **2004**, *3*, 779–782.

18. Yu, M.; Xu, W.; Benjalal, Y.; Barattin, R.; Lægsgaard, E.; Stensgaard, I.; Hliwa, M.; Bouju, X.; Gourdon, A.; Joachim, C.; Linderoth, T. R.; Besenbacher, F. STM Manipulation of Molecular Moulds on Metal Surfaces. *Nano Res.* **2009**, *2*, 254–259.

19. Grill, L.; Rieder, K.-H.; Moresco, F.; Stojkovic, S.; Gourdon, A.; Joachim, C. Controlling the Electronic Interaction Between a Molecular Wire and its Atomic Scale Contacting Pad. *Nano Lett.* **2005**, *5*, 859–863.

20. Savio, L.; Gross, L.; Rieder, K.-H.; Gourdon, A.; Joachim, C.; Moresco, F. Interaction of a Long Molecular Wire With a Nanostructured Surface: Violet Landers on Cu(211). *Chem. Phys. Lett.* **2006**, *428*, 331–337.

21. Grill, L.; Moresco, F.; Jiang, P.; Joachim, C.; Gourdon, A.; Rieder, K.-H. Controlled Manipulation of a Single Molecular Wire Along a Copper Atomic Nanostructure. *Phys. Rev. B* **2004**, *69*, 035416.

22. Savio, L.; Moresco, F.; Gross, L.; Gourdon, A.; Joachim, C.; Rieder, K.-H. Conformations and Controlled Manipulation of a Long Molecular Wire on Cu(111). *Surf. Sci.* **2005**, *585*, 38–46.

23. Alemani, M.; Gross, L.; Moresco, F.; Rieder, K.-H.; Wang, C.; Bouju, X.; Gourdon, A.; Joachim, C. Recording the Intramolecular Deformation of a 4-Legs Molecule During its STM Manipulation on a Cu(211) Surface. *Chem. Phys. Lett.* **2005**, *402*, 180–185.

24. Rosei, F.; Schunack, M.; Jiang, P.; Gourdon, A.; Lægsgaard, E.; Stensgaard, I.; Joachim, C.; Besenbacher, F. Organic Molecules Acting as Templates on Metal Surfaces. *Science* **2002**, *296*, 328–331.

25. Otero, R.; Rosei, F.; Naitoh, Y.; Jiang, P.; Thostrup, P.; Gourdon, A.; Lægsgaard, E.; Stensgaard, I.; Joachim, C.; Besenbacher, F. Nanostructuring Cu Surfaces Using Custom-Designed Molecular Molds. *Nano Lett.* **2004**, *4*, 75–78.

26. Gross, L.; Rieder, K.-H.; Moresco, F.; Stojkovic, S. M.; Gourdon, A.; Joachim, C. Trapping and Moving Metal Atoms With a Six-Leg Molecule. *Nat. Mater.* **2005**, *4*, 892–895.

27. Schunack, M.; Rosei, F.; Naitoh, Y.; Jiang, P.; Gourdon, A.; Lægsgaard, E.; Stensgaard, I.; Joachim, C.; Besenbacher, F. Adsorption Behavior of Lander Molecules on Cu(110) Studied by Scanning Tunneling Microscopy. *J. Chem. Phys.* **2002**, *117*, 6259–6265.

28. Otero, R.; Naitoh, Y.; Rosei, F.; Jiang, P.; Thostrup, P.; Gourdon, A.; Lægsgaard, E.; Stensgaard, I.; Joachim, C.; Besenbacher, F. One-Dimensional Assembly and Selective Orientation of Lander Molecules on an O-Cu Template. *Angew. Chem., Int. Ed.* **2004**, *43*, 2092–2095.

29. Ge, X.; Kuntze, J.; Berndt, R.; Tang, H.; Gourdon, A. Tunneling Spectroscopy of Lander Molecules on Coinage Metal Surfaces. *Chem. Phys. Lett.* **2008**, *458*, 161–165.

30. Kuntze, J.; Ge, X.; Berndt, R. Chiral Structures of Lander Molecules on Cu(100). *Nanotechnology* **2004**, *15*, S337–S340.

31. Gourdon, A. Synthesis of "Molecular Landers. *Eur. J. Org. Chem.* **1998**, 2797–2801.

32. Zambelli, T.; Goudeau, S.; Lagoute, J.; Gourdon, A.; Bouju, X.; Gauthier, S. Molecular Self-Assembly of Jointed Molecules on a Metallic Substrate: From Single Molecule to Monolayer. *ChemPhysChem* **2006**, *7*, 1917–1920.

33. Gross, L.; Moresco, F.; Ruffieux, P.; Gourdon, A.; Joachim, C.; Rieder, K.-H. Tailoring molecular Self-Organization by Chemical Synthesis: Hexaphenylbenzene, Hexa-peri-

hexabenzocoronene, and Derivatives on Cu(111). *Phys. Rev. B* **2005**, *71*, 165428.

34. Stewart, J. J. P. *Mopac*; Stewart Computational Chemistry: Colorado Springs CO, 2007; http://openmopac.net.

35. Xu, W.; Dong, M.; Gersen, H.; Rauls, E.; Vázquez-Campos, S.; Crego-Calama, M.; Reinhoudt, D. N.; Stensgaard, I.; Lægsgaard, E.; Linderoth, T. R.; Besenbacher, F. Cyanuric acid and Melamine on Au(111): Structure and Energetics of Hydrogen-Bonded Networks. *Small* **2007**, *3*, 854–858.

36. Perdigão, L. M. A.; Perkins, E. W.; Ma, J.; Staniec, P. A.; Rogers, B. L.; Champness, N. R.; Beton, P. H. Bimolecular Networks and Supramolecular Traps on Au(111). *J. Phys. Chem. B* **2006**, *110*, 12539–12542.

37. Silly, F.; Shaw, A. Q.; Castell, M. R.; Briggs, G. A. D.; Mura, M.; Martsinovich, N.; Kantorovich, L. Melamine Structures on the Au(111) Surface. *J. Phys. Chem. C* **2008**, *112*, 11476–11480.

38. Mura, M.; Martsinovich, N.; Kantorovich, L. Theoretical Study of Melamine Superstructures and Their Interaction with the Au(111) Surface. *Nanotechnology* **2008**, *1*, 465704.

39. Knaggs, E.; Lonsdale, K.; Wood, R. G.; Williams, G. The Structure of Melamine, $C_3N_6H_6$. *Proc. R. Soc. A* **1940**, *177*, 140–147.

40. Ranganathan, A.; Pedireddi, V. R.; Rao, C. N. R. Hydrothermal Synthesis of Organic Channel Structures: 1:1 Hydrogen-Bonded Adducts of Melamine with Cyanuric and Trithiocyanuric Acids. *J. Am. Chem. Soc.* **1999**, *121*, 1752–1753.

41. Zhang, H.-M.; Xie, Z.-X.; Long, L.-S.; Zhong, H.-P.; Zhao, W.; Mao, B.-W.; Xu, X.; Zheng, L. S. One-Step Preparation of Large-Scale Self-Assembled Monolayers of Cyanuric Acid and Melamine Supramolecular Species on Au(111) Surfaces. *J. Phys. Chem. C* **2008**, *112*, 4209–4218.

42. Barattin, R.; Gourdon, A. Synthesis of Two Complementary Molecular Moulds. *EurJOC* **2009**, 1022–1026.

43. Sadhukhan, S. K.; Viala, C.; Gourdon, A. Syntheses of Hexabenzocoronene Derivatives. *Synthesis* **2003**, *10*, 1521–1525.

44. Lægsgaard, E.; Österlund, L.; Thostrup, P.; Rosmussen, P. B.; Stensgaard, I.; Besenbacher, F. A High-Pressure Scanning Tunneling Microscope. *Rev. Sci. Instrum.* **2001**, *72*, 3537–3542.

45. Sautet, P.; Joachim, C. Calculation of the Benzene on Rhodium Stm Images. *Chem. Phys. Lett.* **1991**, *185*, 23–30.

46. Allinger, N. L.; Chen, K.; Lii, J.-H. An Improved Force Field (MM4) For Saturated Hydrocarbons. *J. Comput. Chem.* **1996**, *17*, 642–668.

47. Lafferentz, L.; Ample, F.; Yu, H.; Hecht, S.; Joachim, C; Grill, L. Conductance of a Single Conjugated Polymer as a Continuous Function of Its Length. *Science* **2009**, *323*, 1193–1197.

48. Manzano, C.; Soe, W.-H.; Wong, H. S.; Ample, F.; Gourdon, A.; Chandrasekhar, N.; Joachim, C. Step-by-Step Rotation of a Molecule-Gear Mounted on an Atomic-Scale Axis. *Nat. Mater.* **2009**, *8*, 576–579.